Phase separation of SARS-CoV-2 nucleocapsid protein with TDP-43 is dependant on C-terminus domains

Michael J Strong *, Crystal McLellan, Brianna Kalpanis, Cristian A Droppelmann, Murray Junop

Posted Date: 4 July 2024

doi: 10.20944/preprints202407.0408.v1

Keywords: neurodegeneration; biomolecular condensates; nucleocapsid protein; RNA binding proteins; amyotrophic lateral sclerosis

Article

Phase Separation of SARS-CoV-2 Nucleocapsid Protein with TDP-43 Is Dependant on C-Terminus Domains

Michael J Strong [1,2,*], Crystal McLellan [1], Brianna Kaplanis [3], Cristian A. Droppelmann [1] and Murray Junop [3]

[1] Molecular Medicine Group, Robarts Research Institute, Schulich School of Medicine & Dentistry, Western University, London, Ontario, Canada
[2] Departments of Clinical Neurological Sciences and Pathology & Laboratory Medicine, Schulich School of Medicine & Dentistry, Western University, London, Ontario, Canada
[3] Department of Biochemistry, Schulich School of Medicine & Dentistry, Western University, London, Ontario, Canada
* Correspondence: mstrong@uwo.ca

Abstract: The SARS-CoV-2 nucleocapsid protein (N protein) is critical to viral replication by undergoing liquid-liquid phase separation to seed the formation of a ribonucleoprotein (RNP) complex to drive viral genomic RNA (gRNA) translation and in also suppressing both stress granules and processing bodies which is postulated to increase uncoated gRNA availability. The N protein can also form biomolecular condensates with a broad range of host endogenous proteins including RNA binding proteins (RBPs). Amongst these RBPs are proteins that are associated with pathological neuronal and glial cytoplasmic inclusions across several adult-onset neurodegenerative disorders, including TAR DNA binding protein 43 kDa (TDP-43) which forms pathological inclusions in over 95% of amyotrophic lateral sclerosis cases. In this study, we demonstrate that the N protein can form biomolecular condensates with TDP-43 and that this is dependant on the N protein C-terminus domain (N-CTD) and the intrinsically disordered C-terminus domain of TDP-43. This process is markedly accelerated in the presence of RNA. In silico modelling suggests that the biomolecular condensate that formed in the presence of RNA is composed of a N protein quadriplex in which the intrinsically disordered TDP-43 C terminus domain is incorporated.

Keywords: neurodegeneration; biomolecular condensates; nucleocapsid protein; RNA binding proteins; amyotrophic lateral sclerosis

Introduction

Although the long term repercussions of the COVID-19 pandemic remain to be fully defined, it is clear that a significant proportion of individuals exposed to the SARS-CoV-2 virus and who develop its clinical correlate COVID-19 will also develop one or more neurological sequelae as a manifestation of the post-COVID condition (PCC) [1–3]. Amongst these consequences, there is growing interest in a potential role for the virus in driving a process of neurodegeneration by participating in pathological biomolecular condensate formation [1,4]. The latter, often manifest as neuronal or glial cytoplasmic inclusions (NCI and GCI, respectively), is a neuropathological correlate to a broad range of adult-onset neurodegenerative disorders that includes amyotrophic lateral sclerosis (ALS), Alzheimer's disease and Parkinson's disease [5–8].

SARS-CoV-2 forms a virion containing its genomic RNA (gRNA) with 4 structural proteins including the spike proteins (S1 & S2 subunits), the membrane protein (M) which facilitates assembly

 doi:10.20944/preprints202407.0408.v1

in the endoplasmic reticulum, the ion channel envelope protein (E protein) and the nucleocapsid protein (N protein). The latter is a RNA binding protein (RBP) that is highly conserved across coronaviruses that assembles with gRNA to form a helical ribonucleoprotein (RNP) complex through its propensity to form biomolecular condensates through liquid-liquid phase separation (LLPS) [9–16]. Encoded by the 9th ORF of the SARS-CoV-2 virus, the N protein is a 46 kDa protein containing 419 amino acid residues that is organized into a N-terminus domain (N-NTD) which contains the primary RNA binding domain (RBD), a C-terminus domain (N-CTD) containing a dimerization domain that is also capable of weaker RNA interactions while being the primary driver of phase separation, and a central Ser/Arg (SR) rich flexible linker region (LKR) with several phosphorylation sites and which also has weak RNA binding capacity (Figure 1) [17–22]. Approximately 40% of the N protein is intrinsically disordered, including intrinsically disordered regions (IDRs) located at the N-terminus (amino acids 1 - 43), the C-terminus (amino acids 365 - 419) and within the LKR (Figure 1) [23]. The N protein self-assembles into higher order oligomeric structures such that two N-terminus domains project from a tight core domain formed by dimerization of the N-CTDs [18]. The N protein dimer undergoes domain compaction by a process in which shorter RNA fragments (< 30 nt) interact only with the N-CTD while longer RNA fragments (>50 – 60 nt) are able to also interact with both N-NTDs and in doing so, drives compaction of the N protein dimer into higher order oligomeric structures which, in the presence of RNA, enhances biomolecular condensate formation [18,24–26].

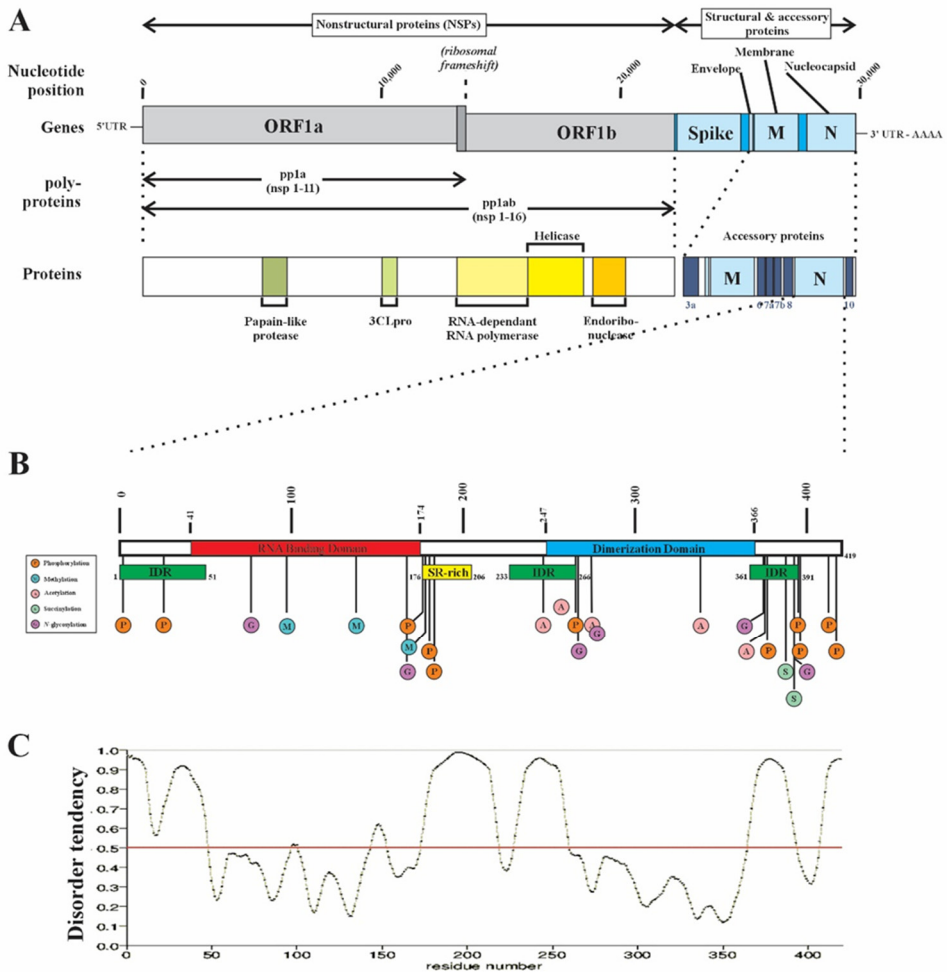

Figure 1. Schematic representation of the SARS-CoV-2 Nucleocapsid protein (N protein). **A.** The structural protein segment of the SARS-CoV-2 gene encodes for multiple proteins, including the spike (S1 & S2 subunits), envelop (E), membrane (M) and nucleocapsid (N) proteins. **B.** The N protein, encoded by the 9th ORF, is a 419 aa protein of 46 kDa composed of three domains: the N-terminus region contains a prominent RNA binding domain (RBD), a C-terminus dimerization domain that

 doi:10.20944/preprints202407.0408.v1

facilitates N protein dimer formation and a Ser/Arg rich central flexible linker region (LKR). The NCP undergoes extensive post-translational modification (PTM), predominantly within IDRs. Note the relative paucity of PTMs in the RBD - a feature not commonly observed in the RBPs of ALS-associated RBPs. Methylation at R95 is required for stress granule formation while F17 has been shown to be the critical interactor for G3PB1 [23,27,28] **C.** The N protein contains three intrinsically disordered domains, including the N and C termini and the LKR (intrinsic disorder tendency predicted using PrDOS (protein disorder prediction system (https://prdos.hcg.jp) and validated with UniProt (https://www.uniprot.org)). Modified from Strong, 2023 [1].

Liquid-liquid phase separation (LLPS) of the N protein is dependant on the N-CTD and can be accelerated by the presence of full-length gRNA as well as homopolymeric RNAs (polyA, polyU, polyC and polyG) [9,13,22,29,30]. Similar to the dynamics described in the context of RBPs in general, higher RNA concentrations suppressed LLPS, consistent with a model of 'reentrant RNA-mediated phase separation". The N protein is extensively phosphorylated in its C-terminus domain while exhibiting minimal RBD posttranslational modifications which is unusual for RBPs [28]. However, the LKR is highly phosphorylated which affects RNA-induced LLPS and nucleocytoplasmic shuttling [12,21].

While the N protein plays a fundamental role in viral RNA replication and transcription through its incorporation in a RNP, it can also induce profound alterations in the immune response by suppressing the PKR-eIF2α-G3BP1/2 pathway of stress granule (SG) formation through direct interactions with the protein kinase PKR and G3BP1 [27,31–33]. Both G3BP1 and TIA-1 are key initiators of the condensation of RNA and proteins into stress granules. By directly interacting with the N-terminus nuclear transport factor 2 (NTF2)-like domain of G3BP1 (residues 11-134), aa F17 of the N protein fundamentally disrupts this assembly - potentially accounting for the significant reduction of SGs in SARS-CoV-2 infected cells [29,31,32,34–37]. When methylated at R95, further suppression of the SG response is observed [27]. While these observations speak to inhibition of the formation of the SG, it has also been suggested that the N protein can induce the disassembly of existent granules [7]. The N protein appears to be unique amongst coronaviruses in also being able to mediate processing body (PB) dissolution, further contributing to impairments in the host stress response in the presence of viral infection [38]. It remains to be determined whether these combined processes lead to the failure of RNA to be sequestrated into either SGs or PBs and thus to enhanced levels of "uncoated" mRNA which can then interact with the N protein to accelerate its phase separation.

Fundamental disturbances in RNA metabolism are a major contributor to the pathophysiology of ALS as evidenced by the presence of pathological glial and neuronal cytoplasmic inclusions (NCIs) of RBPs alongside fundamental alterations in RNA biogenesis [39,40]. A defining feature of RBPs is that they are highly intrinsically disordered, significantly exceeding the degree of intrinsic disorder of other human proteins although their RNA binding domains (RBD) are generally more structured. It is not surprising therefore that NCIs within individual degenerating motor neurons contain multiple RBPs forming heterogeneous fibrils and aggregates [41].

We have postulated that amongst the long-term consequences of SARS-CoV-2 infection, ongoing neuronal expression of the N protein may contribute to pathological biomolecular condensate formation by interaction with other endogenous intrinsically disordered proteins, RNA or with RBPs and thus alter host cell RNA homeostasis [1]. In this study, we have examined how the presence of RNA impacts on the ability of TAR DNA binding protein 43 (TDP-43), the most prevalent ALS-associated RBP observed to be a component of pathological NCIs, to undergo LLPS with the N protein. We have further examined the *in silico*, in vitro and in vivo evidence that suggests that the expression of the N protein in the central nervous system and specifically within neurons could be considered as a pathway of induction of a neurodegenerative disease state. While an attractive postulate, there however remain many unanswered questions as to the mechanism(s) by which the SARS-CoV-2 virus could directly give rise to such disease states.

 doi:10.20944/preprints202407.0408.v1

Results

Protein Aggregation Assay

The ability of SARS-CoV-2 N protein to form protein aggregates in vitro in the presence of RNA and TDP-43 was assessed using an aggregation detection reagent that fluoresces upon binding to non-specific protein aggregates. Aggregation reactions were performed with purified proteins and RNA oligonucleotides in turbidity/crowding buffer immediately before addition to the aggregation detection reagent. Consistent with the observations of others, N protein alone was able to self-aggregate at concentrations of 1-2.5 μM up to 20-25 μM. N protein was then added to either polyrA or polyrG RNA oligos to confirm the reported evidence that RNA stimulates N protein aggregation (Figure 2). The assay determined that when N protein was added to either RNA oligo, protein aggregation was induced above the aggregation level of either RNA alone. PolyrG RNA induced further aggregation of N protein beyond N protein alone.

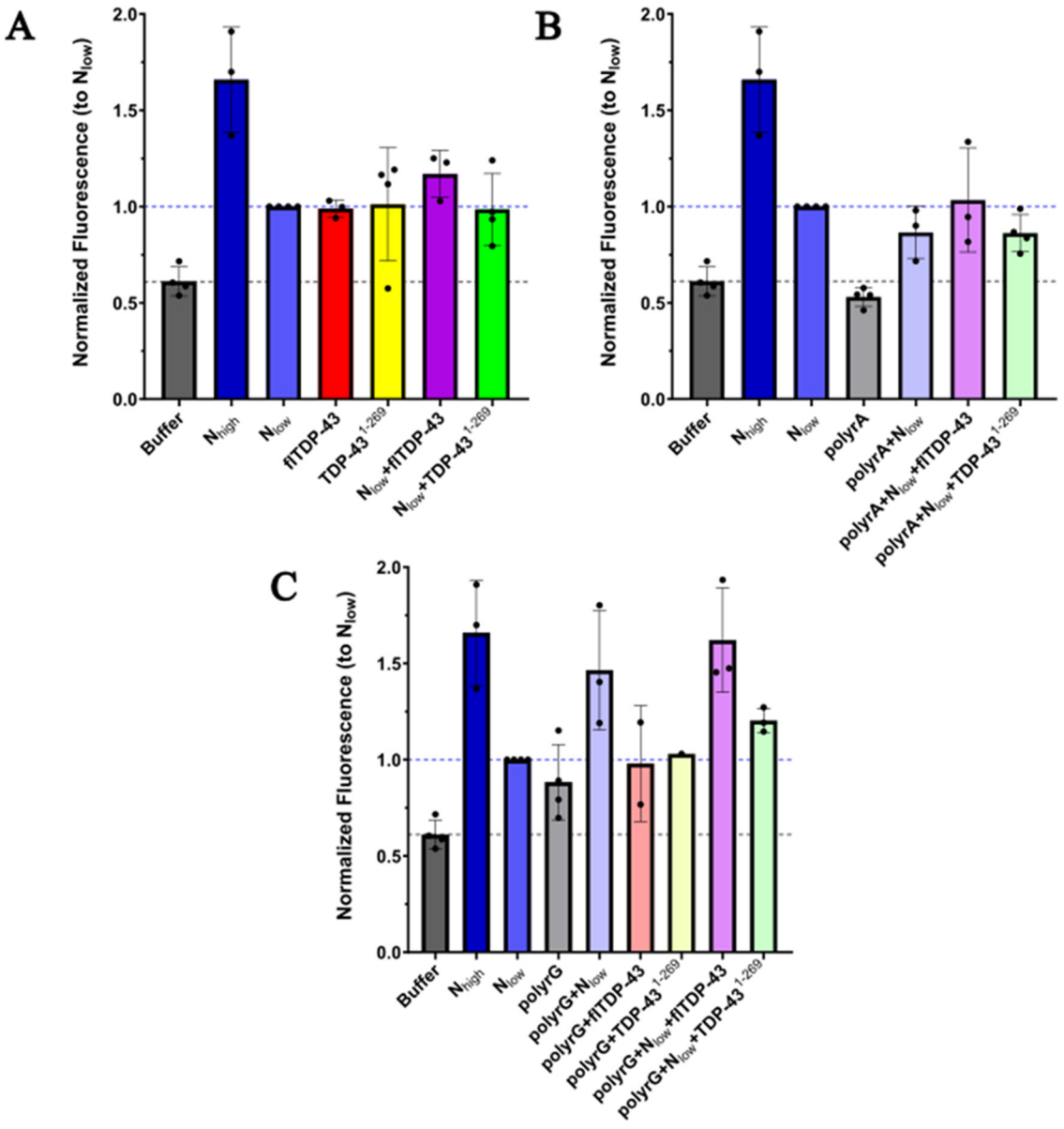

Figure 2. Relative aggregation of purified N and TDP-43 proteins in the absence of RNA (A), in the presence of polyrA (B), or in the presence of polyrG (C). Proteins and/or RNA were mixed at the same time in turbidity buffer with crowding reagent (10% dextran) and added to diluted Proteostat® aggregation detection reagent. Fluorescence shown was recorded with a plate reader approximately

 doi:10.20944/preprints202407.0408.v1

30 minutes after initial mixing. N was mixed with aggregate reagent at a high concentration (20-24 uM) or a low concentration (1-2.5 uM). N and full length TDP-43 (flTDP-43) or N-terminus TDP-43 (TDP-43$^{1-269}$) were mixed at a molar ratio of 1:0.8. N was mixed with the RNA indicated at a molar ratio of 1:0.25. The same molar ratios were used in mixtures containing N, RNA, and TDP-43 variants. Fluorescence was normalized to the low N concentration (N_{low}) used in each experiment. Data include on average three independent experiments.

N protein was also added to either GST-tagged full length or N-terminus TDP-43 (FL-TDP-43 and TDP-43$^{1-269}$, respectively) at a molar ratio of 1:0.8. The presence of these proteins did not significantly change the aggregation status of 1 or 2.5 μM N protein. However, when N protein, polyrA RNA, and FL-TDP-43 were added prior to the aggregation detection, there was an increase in aggregation beyond the level determined for N protein and polyrA alone. An increase in aggregation was also detected when N protein, polyrG, and FL-TDP-43 were mixed, beyond N protein alone. However, the bulk of this aggregation was also detected in the presence of N protein and polyrG. When the TDP-43$^{1-269}$ was used instead of FL-TDP-43 and at a 5-fold higher concentration than FL-TDP-43, aggregation results were similar to when FL-TDP-43 was used, but still attenuated (supplementary Figure S1). When the concentration of TDP-43$^{1-269}$ added to N protein and polyrG was equal to the concentration used for FL-TDP-43, the aggregation level was further attenuated but not increased beyond N protein alone levels. A time course evaluation (50 minutes) did not show re-entry phenomenon for any of the combinations (Supplementary Figure S1).

Together these results confirm that N protein can self-aggregate and that this aggregation is enhanced in the presence of polyrG RNA. In addition, N protein mixed with polyrA RNA and FL-TDP-43 can induce aggregation compared to N protein with polyrA RNA and that the presence of polyrG RNA rather than polyrA RNA further increases this aggregation. However, N protein with polyrG RNA and TDP-43$^{1-269}$ did not induce an increase in aggregation, supporting the notion that the C-terminus domain of TDP-43 is key to N protein TDP-43 molecular condensate induction.

Surface Plasmon Resonance

Surface plasmon resonance (SPR) was used to quantify the in vitro interaction between SARS-CoV-2 N protein and TDP-43. N protein was fixed to a carboxymethyl dextran chip surface as the immobilized ligand and TDP-43 was injected as the potential binding partner. GST-tagged full length TDP-43 or N-terminus TDP-43 were injected onto the chip at the indicated concentrations. The SPR experiments showed a direct interaction between N protein and both the full length TDP-43 and N-terminus TDP-43 with a K_D of 3.78 +/- 0.44 μM and >167 μM, respectively (Figure 3A,B). The interaction between N protein and full length TDP-43 was not dependent on the GST tag as GST alone at concentrations of 2 – 20 μM did not show any interaction with N protein (data not shown). These studies suggest that the TDP-43 C-terminus domain is a major determinant of the interaction between N protein and TDP-43. Unfortunately, this latter domain is soluble in urea but not otherwise, precluding its use in the SPR study.

Preprints.org (www.preprints.org) | NOT PEER-REVIEWED | Posted: 4 July 2024 doi:10.20944/preprints202407.0408.v1

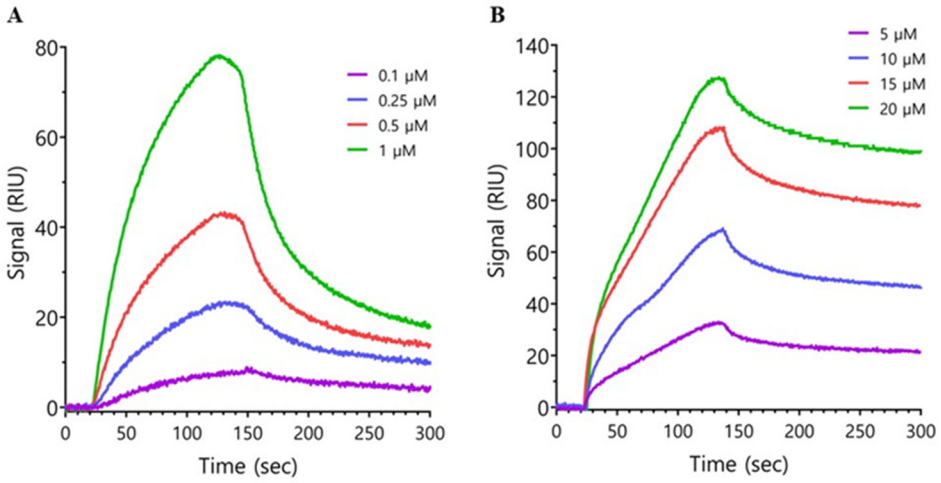

Figure 3. Sensorgrams showing of the interaction of FL-TDP-43 (Figure A) or TDP-43$^{1-269}$ (Figure B) with immobilized SARS-CoV-2 N protein. Protein interactions were assessed by surface plasmon resonance using a Reichert 2SPR, SR7500DC System. Recombinant SARS-CoV-2 N protein was captured on the chip and TDP-43 analyte proteins were serially diluted in running buffer and sensorgrams determined at defined concentrations. K_D values for the interaction with FL-TDP-43 and TDP-43$^{1-269}$ were 3.78 +/- 0.44 µM and >167 µM, respectively, suggesting that the interaction between FL-TDP and N protein is not mediated through the N-terminus domain of TDP-43.

In Silico Modelling of N Protein, TDP-43, and RNA Heteropolymers

To further understand the interaction between the N protein and FL-TDP-43, we used in silico modelling (AlphaFold 3) to evaluate their ability to form biomolecular condensates [42]. When modelling the N protein as a quadriplex in the presence of two FL-TDP-43 proteins, AlphaFold3 predicts a symmetrical complex with TDP-43 positioned more peripherally (Figure 4A). Here RNA binding sites on both proteins appear to be involved in the complex interaction, while the intrinsically disordered C-termini of TDP-43 remained predominately unincorporated (Figure 4A) (supplementary video S1). In contrast, upon addition of either a random 20 mer or 70-mer RNA oligo, condensation occurred with the intrinsically disordered TDP-43 C-terminal domains integrated within the core of the heteropolymer complex, adopting helices in structure (Figure 4B). This was most marked when modelled with the 70-mer oligos in that there appeared to be alignment between TDP-43 C-terminus helices and the RNA binding region within the N-CTD of the N protein, and the 70-mer oligo interwoven throughout (Figure 4C) (supplementary video S2). Meanwhile, the N-terminus RRM1/RRM2 containing domain of TDP-43 appeared to be externally facing and 'cap' the top of the N protein quadriplex. This complex appeared to be more densely compacted compared to the protein complex predictions in the absence of RNA. In summary, the in silico modelling predicts that TDP-43 and N protein will form a complex which in the presence of RNA becomes a more densely packed heteropolymer in which interactions are mediated through the N-CTD and the IDR of the C-terminus of TDP-43.

 doi:10.20944/preprints202407.0408.v1

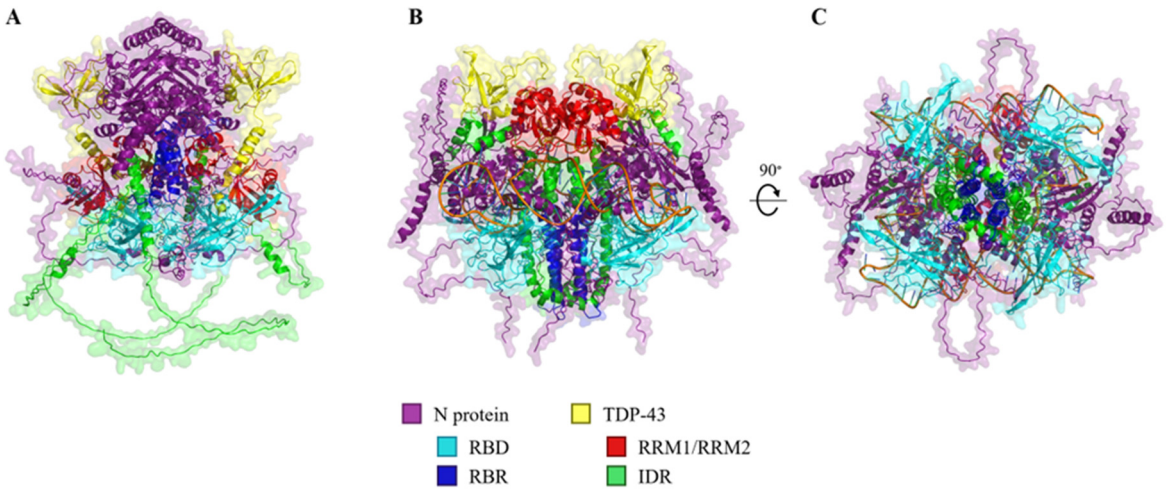

Figure 4. In silico projections of the N protein:TDP-43 heteropolymer complex in the absence or presence of a RNA oligo. **A.** Four N proteins are modeled in complex with two FL-TDP-43 proteins. N protein is displayed in purple, with the N-terminal RNA binding domain (RBD: residues 41-174) in cyan and the C-terminal RNA binding region (RBR: residues 210-246) in blue, respectively. TDP-43 is displayed in yellow, with the RRM1/RRM2 (residues 104-176 & 192-262) in red and the C-terminal intrinsically disordered region (IDR: residues 263-414) in green. **B.** The same complex is modeled in the presence of two random 70-mer RNA oligos. **C.** with a 90° rotation along the x-axis to display a bottom view of the heteropolymer. Note the more compact structure in which the IDR of TDP-43 becomes incorporated in proximity to the N-CTD.

Discussion

We have demonstrated using both in silico projections and co-assembly studies (SPR and aggregation assays) that the N-protein and TDP-43 can, *ex vivo*, form a biomolecular complex. Our SPR data suggests that the C-terminus domain of TDP-43 is the major determinant of the interaction between TDP-43 and the N protein with a K_D for the full-length TDP-43 interaction of 3.78 +/- 0.44 μM whereas that for the isolated N-terminus domain containing both RRMs is greater than 167 μM. In addition, our aggregation data suggests that the presence of RNA will further enhance this process. Given the use of full-length recombinant N protein in our assays, we cannot ascertain whether the interaction is driven by the N-CTD, the N-NTD or the full-length N protein. However, given previous observations regarding the role of RNA in mediating N protein heteropolymer formation [18], the enhancement of the LLPS observed in the aggregations assay in the presence of short RNA oligomers would be consistent with the interaction being dependant on the N-CTD. In silico predictions suggest that this is due to the formation of a complex biomolecular condensate consisting of a N protein quadriplex interacting with the intrinsically disordered domains of two TDP-43 molecules and that this is dependant on the presence of RNA.

The Role of RNA Binding Proteins in Biomolecular Condensate Formation

It is now understood that intracellular LLPS giving rise to membraneless organelles (MLOs) is a critical physiological process that results in the formation of dynamic, highly functional biomolecular condensates. In contrast to more classical canonical macromolecular particles (e.g., RNA), biomolecular condensates are highly dynamic and readily exchange components with their surroundings, in part due to the relatively weak, non-covalent nature of interactions within the condensates [43]. They can range from 20 nm (i.e., interchromatin granules) to 1-6 μm (i.e., P bodies) in diameter [44]. Because of the fluidity of their composition, biomolecular condensates can display regions of differing composition and density, potentially underlying their ability to drive independent processes within the same condensate [45].

 doi:10.20944/preprints202407.0408.v1

The most prevalent biomolecular condensates are combined RNA and protein assemblies (ribonucleoprotein (RNP) granules, or RNP bodies) such as SGs and PBs where assembly/disassembly is driven by the phase separation process. Also included in this grouping are nucleoli, nuclear paraspeckles, Cajal bodies, transport granules as well as Balbiani bodies [46]. Key physiological functions of biomolecular condensates include major aspects of RNA metabolism, including transcription, pre-mRNA processing, subcellular localization and the regulation of translation and decay [44,47].

The process of biomolecular condensation is divided into two broad categories of participating proteins: scaffold proteins that drive reversible condensate formation or clients which are proteins that preferentially partition into condensates [48]. The predominant proteins found within biomolecular condensates are RNA binding proteins (RBPs), a class of *trans*-acting regulatory proteins that interact with *cis*-acting RNA elements with their greatest specificity being for mRNA elements [49,50]. RBPs interact with cognate transcripts through a small repertoire of RNA-binding domains (RBDs) that include RNA recognition motifs (RRM; typically, an average of 90 amino acids with 2 α-helices against an antiparallel β sheet), K homology (KH, a highly conserved protein domain of approximately 70 amino acids that interacts with either ssRNA or ssDNA), arginine-glycine-glycine (RGG) motifs, zinc-finger (ZnF; family of proteins averaging 30 aa with a $\beta\beta\alpha$ topology) and DEAD/DEAH box helicase) [51,52]. The combination of consecutive RRMs in an RBP increases binding affinity and specificity. In this model, we propose that the N protein is the scaffold protein which seeds a quadriplex structure in which TDP-43 is the client protein.

These observations have broader implications for a putative role for the interaction of the N protein and RBPs in the genesis of pathological biomolecular condensates in neurodegeneration. RBPs play a critical role in mRNA biogenesis, including transcription, pre-mRNA processing, localization, translation and decay [44]. RBPs share a core set of common features that may contribute to their propensity to participate in pathological inclusion formation including their enrichment in IDRs, significantly more so than other human proteins. Within any given RBP, using prediction algorithms, the RBD is more likely to be structured (a lower predicted ID of 0.03 – 0.05) compared to the non RBD regions (a higher predicted ID of 0.30 – 0.40) and to be enriched with post-translational modifications [53]. *Cis*-acting mRNA elements are not unique to an individual *trans*-acting RBP and thus multiple mRNA partners for a single RBP and multiple RBPs can interact with a single RNA (through multiple *cis*-acting elements).

Our study does not account for the significant impact that post-translational modifications (PTMs) of either N protein or TDP-43 will have upon the dynamics of biomolecular condensate formation. Using mass spectroscopy on in vivo cross linked RNA-protein interactors, it has been shown that RBPs are highly modified by PTMs as a class of proteins and significantly greater than that observed for the larger human protein database [50]. Given that RBPs are also significantly more intrinsically disordered that other protein classes and thus more flexible (or less rigid), this suggests that PTMs contribute to the dynamic regulatory roles of RBPs. In addition, a single RBP may contain multiple RBDs which can assist in co-ordinating and enhancing mRNA binding. Moreover, the presence of a RBD and IDR in a RBP increases the propensity for LLPS. The characteristics are readily observed in RBPs that are commonly observed to be incorporated in pathological biomolecular condensates observed in a broad range of neurodegenerative disorders, such as the RBPs TDP-43, FUS/TLS, EWS, and RBM45 that are key to the pathological NCIs of ALS [54,55].

The key driving force for LLPS are interactions between aromatic and +ve charged amino acids (ie., lysine, arginine and histidine) while glycine enhances fluidity with glutamine and serine promoting hardness [46]. Proteins that undergo LLPS tend to harbour intrinsically disordered regions (IDRs) or coiled-coil domains which increase self-interaction and aggregation at higher concentrations. IDRs are composed of long stretches of low amino acid diversity lacking in hydrophobic residues (low complexity domains; LCDs) which typically mediate cooperative folding [56]. Although occasionally referred to as prion-like domains (PrLDs), PrDLs are most appropriately considered as a subset of IDRs with similarities to yeast prion proteins with enrichment in glutamine and/or asparagine residues. Typically, amino acids found within LCDs include polar (glutamine and

 doi:10.20944/preprints202407.0408.v1

serine) and aromatic (tyrosine) residues. Tyrosine residues generally combine with glycine and serine in forming [G/S]Y[G/S] motifs which have a tendency to form aggregates *in vitro*, lack well-defined 3D structures and favour the formation of hydrogels [44,57]. IDRs also generally consist of repeats of arginine/serine (RS repeat), arginine/glycine (RGG box), arginine or lysine-rich patches (R/K patches).

While IDRs are the main drivers of LLPS, there are examples of non-prion like domains that drive LLPS. IDRs can also be the sole RBD in a RBP. Because of their lack of structure, IDRs can co-ordinate RNA binding in concert with other domains and demonstrate a range of specificities from high to nonselective and may promote protein-RNA co-folding upon interaction with target RNAs [48,57]. At low RNA:RBP stoichiometry, the RNAs will facilitate RBP phase separation whereas a high RNA:RBP stoichiometry leads to soluble RNP formation [58]. Of note, proteins that are highly prone to condensate formation possess both RBDs and IDRs and can act as nucleating centres for increased condensate formation and potentially pathological liquid-solid phase separation (LLPS), thus giving rise to the hallmark nuclear and cytoplasmic inclusions of many neurodegenerative disorders. Biomolecular condensates tend to be enriched in proteins that have dual RNA binding ability and IDRs, with an increased number of RBDs correlating with a greater propensity to phase separate [45].

In the context of pathological biomolecular condensate formation, it is noteworthy that a number of RBPs lack a classical RBD but instead interact with RNA through an IDR. There is increasing evidence that IDRs can drive RNA/RBP interactions with a higher affinity to RNA for RBPs that contain ordered RBDs and which can transition to structured domains upon RNA binding [52]. As such, RBPs participate in LLPS through RBDs, IDRs and (as will be discussed) through an array of post-translational modifications (PTMs).

RBP Post-Translational Modifications as Modulators of Biomolecular Condensates

PTMs are important to tuning intermolecular interactions through regulating the charge state of IDPs and thus can while capable of regulating LLPS or biomolecular condensate genesis, can also promote liquid-solid phase shift LSPS and 'molecular hardening" [46]. PTMs can lead to the weakening or enhancement of multivalent interactions in biomolecular condensates, and, through either recruiting or excluding macromolecules to the complex, modulate the physical state of the complex. The most well characterized RBP PTMs are those related to cellular distribution and interactions, in particular with RNA through modulating RNA binding properties: phosphorylation, acetylation, arginine methylation, sumoylation, while ubiquitinylation is involved with degradation and turnover; phosphorylation and methylation being key for RNA interactions (with potential opposing interactions) [51]. RBP PTMs influence RNA biogenesis by impacting on subcellular localization (e.g., nuclear import), stability, degradation & translation (thru regulating alternative splicing or polyadenylation), modulation of interactions with RNA and other proteins and by modulate their propensity for LLPS (an example is that methylation may preclude phosphorylation at an adjacent site by steric hindrance) [51]. An important role for RBP PTMs is increasingly evident across a range of human diseases, including cancer & neurodegeneration; relevance to ALS of TDP-43, FUS/TLS and hnRNP-A/B [46];

Evidence That the N-Protein Can Be Involved in Pathological Biomolecular Condensate Formation Relevant to Human Neurodegenerative Disease States

The postulate that a viral infection may set forward a cascade of events that can give rise to, accelerate, or be associated with an increased prevalence of neurodegenerative processes is not entirely novel [59–61].

Neuropathological studies of individuals dying during the *acute* manifestations of COVID-19 or shortly thereafter demonstrate prominent neuroinflammatory changes with the presence of SARS-CoV-2 RNA or the expression of either S or N proteins by immunohistological evidence being inconsistent and, when present, not clearly correlated with the severity of the neuroinflammatory pathology [62–65]. Neuropathological features of a hypoxic-ischemic injury often accompanied by vascular pathology with infarction alongside evidence of immune-mediated microvascular

 doi:10.20944/preprints202407.0408.v1

pathology and blood-brain barrier compromise in the acute stages of COVID-19 have been well documented [66–69]. The presence of diffuse microglial activation in the brainstem including microglial nodules, astrogliosis, and perivascular inflammation with parenchymal CD3+ and CD8+ T cells further supports the concept that the acute neurological manifestations of COVID-19 are the consequence of a prominent neuroinflammatory process in the absence of robust evidence of ongoing SARS-CoV-2 infection of the brain [65,70–72].

The question of whether the SARS-CoV-2 virus or N protein can *chronically* be expressed in the human central nervous system and more specifically neurons as opposed to non-neuronal cell populations remains entirely uncertain. In vitro studies using the OC34 strain of the human coronavirus (HCoV-OC43) in primary murine hippocampal and cortical neuron-enriched cultures demonstrated that neurons were preferentially targeted by the virus, although at later timepoints, astrocytes were also infected [73]. Infected neurons had largely disappeared by day 7 post infection. Human IPSC-derived motor neurons have been shown to be susceptible to SARS-CoV-2 infection and although the levels of viral replication were low, infection could be passaged to VeroE6 cells using supernatant derived from the infected IPSC-derived motor neurons [74]. Of specific relevance to our work, N protein expression was detected in SARS-CoV-2 infected neurons. In vivo studies using intracerebral inoculums in BALB/c mice were associated with a progressive motor dysfunction with prominent neuronal degeneration. Macaques examined 5 to 6 weeks post SARS-CoV-2 inoculation and thus beyond the acute stages of infection demonstrated an ongoing neuroinflammatory response with microglial nodules, microglial activation, meningeal inflammation and T-cell infiltrates within the brain parenchyma [75]. Active viral replication at this time point was not observed. Of importance to this discussion, α-synuclein aggregates in the ventral midbrain of 6 of the 8 macaques studied were also observed. Although this latter study did not examine the colocalization of α-synuclein aggregates with either the SARS-CoV-2 or N protein, the ability of both the S1 and N proteins (in particular the N-CTD domain) to interact with α-synuclein, the main component of Parkinson's disease associated Lewy bodies, and accelerate pathological fibril formation, has been demonstrated by both bioinformatics approaches and in vitro [76–78].

It remains to be resolved whether the N protein can be chronically expressed in *human* brain or spinal cord and in doing so be available to either initiate or accelerate pathological biomolecular condensates with candidate RBPs. Although in PCC persistence of SARS-COV-2 RNA and both the S and N proteins has been documented, including in plasma neuron-derived exosomes for upwards of 16 months post COVID-19, there are no studies correlating this with features of neurodegeneration [79,80]. There remains controversy as to whether the SARS-CoV-2 virus can directly infect human neurons or whether the neurological complications of virus exposure is the cumulative impact of multiple pathological processes. Recent in vitro evidence supports that the SARS-CoV-2 virus can directly infect astrocytes which then function as the primary viral reservoir capable of mediating neuronal injury [81].

In the context of a potential role for the N protein in inducing pathological oligomers with ALS-associated RBPs, as demonstrated here and elsewhere, there is clear ex vivo evidence that such a process can occur. It is noteworthy that the protein interactome of N protein is enriched for proteins associated with SGs, including several (e.g., G3BP1/2, Stau1 and Caprin1) that are associated with the pathophysiology of ALS [27,82–86]. Whether pathological LLPS or LSPS driven by the N protein occurs in the human nervous system and can be incriminated in the proposed increase in prevalence of neurodegenerative diseases post COVID-19 awaits further evidence from both longitudinal case control studies and detailed neuropathological analysis. Moreover, whether this process is determined by direct in vivo exposure of neurons to the SARS-CoV-2 virus or the N protein directly awaits similar studies.

Conclusion

It has been well established that the SARS-CoV-2 N protein shares many features with classical RBPs and in doing so can form both homopolymeric structures in addition to heteropolymeric oligomers as drivers to biomolecular condensates. Using a wide range of methodologies, including

 doi:10.20944/preprints202407.0408.v1

in silico projections, ex vivo studies, in vitro cell culture methodologies and in vivo experimental paradigms, there is substantive evidence that the N protein can undergo pathological LLPS in which endogenous RBPs are incorporated into biomolecular condensates (Figure 5). However, it is less clear whether these observations can be extended into a causation of chronic neurodegeneration in which the hallmark is the presence of pathological neuronal and glial cytoplasmic inclusions and in which the N protein would be postulated to be a major driver of pathological biomolecular condensates. Many questions remain before the validity of such a hypothesis can be addressed, including whether there is a natural cellular 'reservoir' for SARS-CoV-2 or N protein within the central nervous system. And if such a reservoir exists and is non-neuronal, how the N protein might be propagated into neurons and having done so, whether it can then propagate pathological biomolecular condensates. Further, whether such propagation is directly linked to the development of a chronic degenerative disease state. Answering these questions in the wake of the COVID-19 pandemic is a critical next step to understanding how to mitigate the projected increase in these disease states, including ALS.

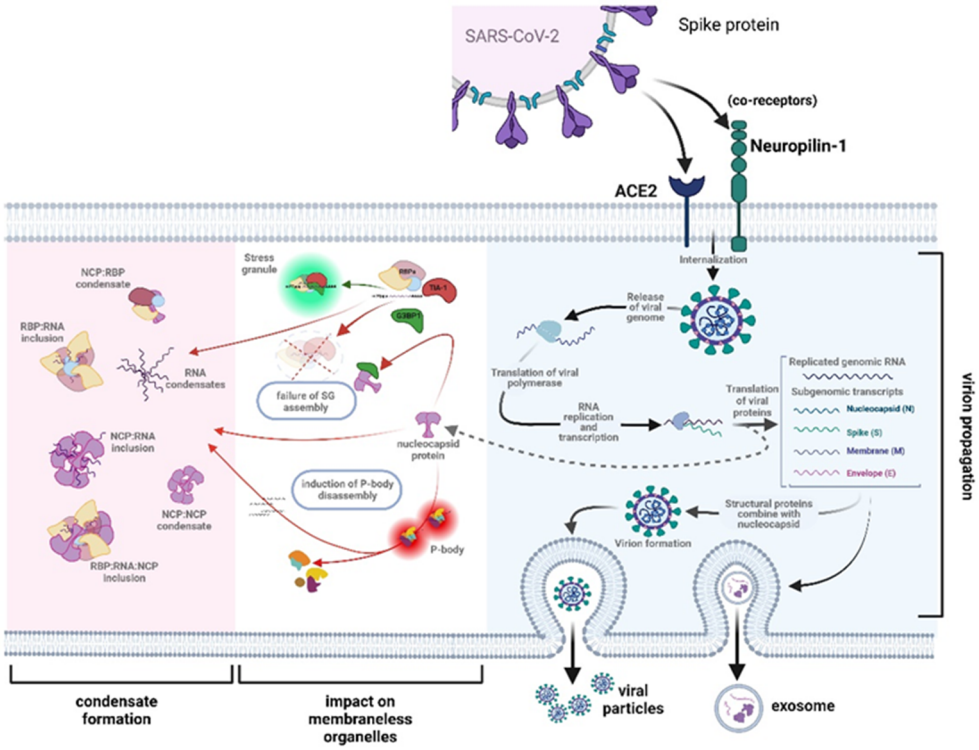

Figure 5. Schematic of role of the SARS-CoV-2 nucleocapsid protein (N-protein) in driving pathological biomolecular condensate formation. Upon endocytosis of the SARS-CoV-2 virus and release of the viral genome, the N protein plays a critical role in the translation of the viral gRNA and the formation of the virion. The latter is released either through exocytosis or encapsulated in exosomes. However, the free N protein also inhibits the formation of stress granules (SGs) by directly interacting with G3BP1 which is critical to the initial assembly of the SG. Not shown is the proposed additive role of N protein in leading to the disassembly of processing bodies (PB). The net effects is the formation of pathological biomolecular condensates of varying composition: N protein homopolymers; N protein:RNA heteropolymers; N protein: RBP heteropolymers; and, N protein:RNA:RBP heteropolymers. It is hypothesized that any or all of these pathological molecular condensates would play a critical role in the pathogenesis of neuronal or glial cytoplasmic inclusions that are the neuropathological hallmark of a broad array of neurodegenerative disorders (figure modified from Strong, 2023 [1] and created with BioRender.com).

 doi:10.20944/preprints202407.0408.v1

Materials & Methods

Protein Aggregation Assay

Protein aggregation in the presence of SARS-CoV-2 N protein, TDP-43 proteins, and short RNA oligos was assessed with the PROTEOSTAT® Protein Aggregation Assay (Enzo). Commercially available N protein (GenScript) was concentrated ~10-fold and the storage buffer exchanged for 1xPBS using Pierce™ Protein Concentrators PES 10K (ThermoScientific) according to the manufacturer's directions. TDP-43 proteins used in this experiment included GST-tagged full length TDP-43 (consisting of amino acids 1-414 of TDP-43) (generously donated from Emanuele Buratti's group) or N-terminus TDP-43 (consisting of amino acids 1-269), including both the RRM1 and RRM2 RNA-binding domains, purified as previously published [87]. Frozen TDP-43 aliquots were concentrated and the storage buffer exchanged to 1xPBS similarly to N protein. Final protein concentrations were determined by BCA microplate assay with BSA as standards. PolyrG and polyrA RNA oligos used in the aggregation assays were synthesized by MilliporeSigma and consisted of the sequences 5′-GGGGGGUGGGGGUGGGGG-3′ and 5′-AAAAAAAAAAAAAAAAAA-3′ respectively. PROTEOSTAT® detection reagent was mixed according to the manufacturer's directions for the volume required. Proteins and/or RNA were gently mixed at the concentrations and molar ratios indicated in turbidity/crowding buffer consisting of Tris-HCl, NaCl, 0.5 mM DTT and 10% dextran, then 98 µl of each reaction mixture was quickly mixed with 2 µl of detection reagent pre-loaded in a 96-well black-walled microplate in duplicate. Positive and negative aggregation standards were included and buffer only was used as a control. Microplates were read with an excitation setting of 550 nm and emission of 600 nm every 2 minutes for 50 minutes in a BioTek Synergy H1 microplate reader.

Surface Plasmon Resonance

Protein interactions were assessed using a Reichert 2SPR, SR7500DC System. Standard amine coupling (EDC/NHS chemistry) was used to capture commercially available recombinant SARS-CoV-2 N protein on a carboxymethyl dextran hydrogel sensor chip (Reichert). The concentration of N protein used for immobilization was 100 ug/ml and the amount of ligand immobilized was approximately 5000 µRIU. TDP-43 analyte proteins (either GST-tagged full length TDP-43 or the N-terminus domain containing both the RRM1 and RRM2 domains) were serially diluted to the concentrations indicated in running buffer (10 mM Hepes pH 7.5, 150 mM NaCl, and 0.1% Tween-20). Analyte concentrations of 0.1 –1 µM of FL-TDP-43 or 5 – 20 µM N-terminus TDP-43 (TDP-43$^{1\text{-}269}$) were injected on both the ligand and reference channels at 35 µl/min for 2 minutes with a 3-minute dissociation time at 22 °C. GST protein (2, 10 and 20 µM) was injected to evaluate possible unspecific binding of the GST-tag on full length TDP-43 to immobilized N protein. Buffer injections were used as blanks for the experiments. Sensorgram analysis and dissociation constant (K_D) calculations were performed using Reichert SPRAutolink (version 1.1.16), TraceDrawer (version 1.8.1), and GraphPad Prism 9.5 software packages.

In Silico Modelling of the N Protein, TDP-43 and RNA Interactions

In silico molecular modelling of the N protein, TDP-43 and RNA interactions were conducted using AlphaFold 3 to generate projections of N protein heteropolymers [42]. AlphaFold input parameters included four copies of the full-length sequence for TDP-43 (Uniprot accession code: Q13148), and two copies of the full-length sequence for the N protein (Uniprot accession code: P0DTC9), where highest ranking models were selected for further investigation. Ribonucleoprotein complex formation was simulated under these parameters alongside two copies a 70-mer RNA oligo (5′-GUCGCAGAUUAUGGGUUUACGAUCCGACCUACAAGUUCCGGCCCCCUGUGGUAACCCG CACGCAUUAGGU-3′), derived from Molbiotools random sequence generator (https://molbiotools.com/randomsequencegenerator.php) with the input RNA parameters specifying a length of 70, and 50% for GC content.

Author Contributions: Conceptualization, M.J.S., C.M., and B.K.; Methodology, M.J.S., C.M., and B.K.; Formal Analysis, M.J.S., C.M., B.K., and C.D.; Investigation, C.M., and B.K.; Resources, M.J.S.; Writing—Original Draft Preparation, M.J.S.; Writing—Review & Editing, M.J.S., C.M., B.K., C.D., and M.J.; Supervision, M.J.S.; Project Administration, M.J.S.; Funding Acquisition, M.J.S.

Funding: Research funding provided by an operating grant from the Canadian Institutes of Health Research (CIHR grant #201806SOP-411481) and by a generous donation from the Temerty Family Foundation.

Institutional review board statement: not applicable.

Data availability statement: The original contributions presented in the study are included in the article/supplementary material, further inquiries can be directed to the corresponding author/s.

Acknowledgments: not applicable.

Conflicts of interest: The authors declare no conflicts of interest.

References

1. Strong, M.J. SARS-CoV-2, aging, and Post-COVID-19 neurodegeneration. *J Neurochem* **2023**, *165*, 115-130, doi:10.1111/jnc.15736.
2. Pattanaik, A.; Bhandarkar, B.S.; Lodha, L.; Marate, S. SARS-CoV-2 and the nervous system: current perspectives. *Arch Virol* **2023**, *168*, 171, doi:10.1007/s00705-023-05801-x.
3. Xu, E.; Xie, Y.; Al-Aly, Z. Long-term neurologic outcomes of COVID-19. *Nat Med* **2022**, *28*, 2406-2415, doi:10.1038/s41591-022-02001-z.
4. Hammarstrom, P.; Nystrom, S. Viruses and amyloids - a vicious liaison. *Prion* **2023**, *17*, 82-104, doi:10.1080/19336896.2023.2194212.
5. Tsoi, P.S.; Quan, M.D.; Ferreon, J.C.; Ferreon, A.C.M. Aggregation of Disordered Proteins Associated with Neurodegeneration. *Int J Mol Sci* **2023**, *24*, doi:10.3390/ijms24043380.
6. Hurtle, B.T.; Xie, L.; Donnelly, C.J. Disrupting pathologic phase transitions in neurodegeneration. *J Clin Invest* **2023**, *133*, doi:10.1172/JCI168549.
7. Li, Y.; Lu, S.; Gu, J.; Xia, W.; Zhang, S.; Zhang, S.; Wang, Y.; Zhang, C.; Sun, Y.; Lei, J.; et al. SARS-CoV-2 impairs the disassembly of stress granules and promotes ALS-associated amyloid aggregation. *Protein Cell* **2022**, *13*, 602-614, doi:10.1007/s13238-022-00905-7.
8. Campos-Melo, D.; Hawley, Z.C.E.; Droppelmann, C.A.; Strong, M.J. The Integral Role of RNA in Stress Granule Formation and Function. *Front Cell Dev Biol* **2021**, *9*, 621779, doi:10.3389/fcell.2021.621779.
9. Perdikari, T.M.; Murthy, A.C.; Ryan, V.H.; Watters, S.; Naik, M.T.; Fawzi, N.L. SARS-CoV-2 nucleocapsid protein phase-separates with RNA and with human hnRNPs. *EMBO J* **2020**, *39*, e106478, doi:10.15252/embj.2020106478.
10. Chang, C.K.; Hou, M.H.; Chang, C.F.; Hsiao, C.D.; Huang, T.H. The SARS coronavirus nucleocapsid protein--forms and functions. *Antiviral Res* **2014**, *103*, 39-50, doi:10.1016/j.antiviral.2013.12.009.
11. Tilocca, B.; Soggiu, A.; Sanguinetti, M.; Musella, V.; Britti, D.; Bonizzi, L.; Urbani, A.; Roncada, P. Comparative computational analysis of SARS-CoV-2 nucleocapsid protein epitopes in taxonomically related coronaviruses. *Microbes Infect* **2020**, *22*, 188-194, doi:10.1016/j.micinf.2020.04.002.
12. Bai, Z.; Cao, Y.; Liu, W.; Li, J. The SARS-CoV-2 Nucleocapsid Protein and Its Role in Viral Structure, Biological Functions, and a Potential Target for Drug or Vaccine Mitigation. *Viruses* **2021**, *13*, doi:10.3390/v13061115.
13. Rak, A.; Isakova-Sivak, I.; Rudenko, L. Overview of Nucleocapsid-Targeting Vaccines against COVID-19. *Vaccines (Basel)* **2023**, *11*, doi:10.3390/vaccines11121810.
14. Marra, M.A.; Jones, S.J.; Astell, C.R.; Holt, R.A.; Brooks-Wilson, A.; Butterfield, Y.S.; Khattra, J.; Asano, J.K.; Barber, S.A.; Chan, S.Y.; et al. The Genome sequence of the SARS-associated coronavirus. *Science* **2003**, *300*, 1399-1404, doi:10.1126/science.1085953.
15. Rota, P.A.; Oberste, M.S.; Monroe, S.S.; Nix, W.A.; Campagnoli, R.; Icenogle, J.P.; Penaranda, S.; Bankamp, B.; Maher, K.; Chen, M.H.; et al. Characterization of a novel coronavirus associated with severe acute respiratory syndrome. *Science* **2003**, *300*, 1394-1399, doi:10.1126/science.1085952.
16. Luo, H.; Chen, Q.; Chen, J.; Chen, K.; Shen, X.; Jiang, H. The nucleocapsid protein of SARS coronavirus has a high binding affinity to the human cellular heterogeneous nuclear ribonucleoprotein A1. *FEBS Lett* **2005**, *579*, 2623-2628, doi:10.1016/j.febslet.2005.03.080.
17. Kang, S.; Yang, M.; Hong, Z.; Zhang, L.; Huang, Z.; Chen, X.; He, S.; Zhou, Z.; Zhou, Z.; Chen, Q.; et al. Crystal structure of SARS-CoV-2 nucleocapsid protein RNA binding domain reveals potential unique drug targeting sites. *Acta Pharm Sin B* **2020**, *10*, 1228-1238, doi:10.1016/j.apsb.2020.04.009.
18. Ribeiro-Filho, H.V.; Jara, G.E.; Batista, F.A.H.; Schleder, G.R.; Costa Tonoli, C.C.; Soprano, A.S.; Guimaraes, S.L.; Borges, A.C.; Cassago, A.; Bajgelman, M.C.; et al. Structural dynamics of SARS-CoV-2 nucleocapsid protein induced by RNA binding. *PLoS Comput Biol* **2022**, *18*, e1010121, doi:10.1371/journal.pcbi.1010121.

19. McBride, R.; van Zyl, M.; Fielding, B.C. The coronavirus nucleocapsid is a multifunctional protein. *Viruses* **2014**, *6*, 2991-3018, doi:10.3390/v6082991.
20. Surjit, M.; Lal, S.K. The SARS-CoV nucleocapsid protein: a protein with multifarious activities. *Infect Genet Evol* **2008**, *8*, 397-405, doi:10.1016/j.meegid.2007.07.004.
21. Savastano, A.; Ibanez de Opakua, A.; Rankovic, M.; Zweckstetter, M. Nucleocapsid protein of SARS-CoV-2 phase separates into RNA-rich polymerase-containing condensates. *Nat Commun* **2020**, *11*, 6041, doi:10.1038/s41467-020-19843-1.
22. Estelle, A.B.; Forsythe, H.M.; Yu, Z.; Hughes, K.; Lasher, B.; Allen, P.; Reardon, P.N.; Hendrix, D.A.; Barbar, E.J. RNA structure and multiple weak interactions balance the interplay between RNA binding and phase separation of SARS-CoV-2 nucleocapsid. *PNAS Nexus* **2023**, *2*, pgad333, doi:10.1093/pnasnexus/pgad333.
23. Tenchov, R.; Zhou, Q.A. Intrinsically Disordered Proteins: Perspective on COVID-19 Infection and Drug Discovery. *ACS Infect Dis* **2022**, *8*, 422-432, doi:10.1021/acsinfecdis.2c00031.
24. Wu, W.; Cheng, Y.; Zhou, H.; Sun, C.; Zhang, S. The SARS-CoV-2 nucleocapsid protein: its role in the viral life cycle, structure and functions, and use as a potential target in the development of vaccines and diagnostics. *Virol J* **2023**, *20*, 6, doi:10.1186/s12985-023-01968-6.
25. Cubuk, J.; Alston, J.J.; Incicco, J.J.; Singh, S.; Stuchell-Brereton, M.D.; Ward, M.D.; Zimmerman, M.I.; Vithani, N.; Griffith, D.; Wagoner, J.A.; et al. The SARS-CoV-2 nucleocapsid protein is dynamic, disordered, and phase separates with RNA. *Nat Commun* **2021**, *12*, 1936, doi:10.1038/s41467-021-21953-3.
26. Wang, Y.; Ling, X.; Zhang, C.; Zou, J.; Luo, B.; Luo, Y.; Jia, X.; Jia, G.; Zhang, M.; Hu, J.; et al. Modular characterization of SARS-CoV-2 nucleocapsid protein domain functions in nucleocapsid-like assembly. *Mol Biomed* **2023**, *4*, 16, doi:10.1186/s43556-023-00129-z.
27. Cai, T.; Yu, Z.; Wang, Z.; Liang, C.; Richard, S. Arginine methylation of SARS-Cov-2 nucleocapsid protein regulates RNA binding, its ability to suppress stress granule formation, and viral replication. *J Biol Chem* **2021**, *297*, 100821, doi:10.1016/j.jbc.2021.100821.
28. Sun, Z.; Zheng, X.; Ji, F.; Zhou, M.; Su, X.; Ren, K.; Li, L. Mass Spectrometry Analysis of SARS-CoV-2 Nucleocapsid Protein Reveals Camouflaging Glycans and Unique Post-Translational Modifications. *Infect Microbes Dis* **2021**, *3*, 149-157, doi:10.1097/IM9.0000000000000071.
29. Lu, S.; Ye, Q.; Singh, D.; Cao, Y.; Diedrich, J.K.; Yates, J.R., 3rd; Villa, E.; Cleveland, D.W.; Corbett, K.D. The SARS-CoV-2 nucleocapsid phosphoprotein forms mutually exclusive condensates with RNA and the membrane-associated M protein. *Nat Commun* **2021**, *12*, 502, doi:10.1038/s41467-020-20768-y.
30. Iserman, C.; Roden, C.A.; Boerneke, M.A.; Sealfon, R.S.G.; McLaughlin, G.A.; Jungreis, I.; Fritch, E.J.; Hou, Y.J.; Ekena, J.; Weidmann, C.A.; et al. Genomic RNA Elements Drive Phase Separation of the SARS-CoV-2 Nucleocapsid. *Mol Cell* **2020**, *80*, 1078-1091 e1076, doi:10.1016/j.molcel.2020.11.041.
31. Yang, Z.; Johnson, B.A.; Meliopoulos, V.A.; Ju, X.; Zhang, P.; Hughes, M.P.; Wu, J.; Koreski, K.P.; Clary, J.E.; Chang, T.C.; et al. Interaction between host G3BP and viral nucleocapsid protein regulates SARS-CoV-2 replication and pathogenicity. *Cell Rep* **2024**, *43*, 113965, doi:10.1016/j.celrep.2024.113965.
32. Zheng, Z.Q.; Wang, S.Y.; Xu, Z.S.; Fu, Y.Z.; Wang, Y.Y. SARS-CoV-2 nucleocapsid protein impairs stress granule formation to promote viral replication. *Cell Discov* **2021**, *7*, 38, doi:10.1038/s41421-021-00275-0.
33. Luo, L.; Li, Z.; Zhao, T.; Ju, X.; Ma, P.; Jin, B.; Zhou, Y.; He, S.; Huang, J.; Xu, X.; et al. SARS-CoV-2 nucleocapsid protein phase separates with G3BPs to disassemble stress granules and facilitate viral production. *Sci Bull (Beijing)* **2021**, *66*, 1194-1204, doi:10.1016/j.scib.2021.01.013.
34. Dolliver, S.M.; Kleer, M.; Bui-Marinos, M.P.; Ying, S.; Corcoran, J.A.; Khaperskyy, D.A. Nsp1 proteins of human coronaviruses HCoV-OC43 and SARS-CoV2 inhibit stress granule formation. *PLoS Pathog* **2022**, *18*, e1011041, doi:10.1371/journal.ppat.1011041.
35. Kim, D.; Maharjan, S.; Kang, M.; Kim, J.; Park, S.; Kim, M.; Baek, K.; Kim, S.; Suh, J.G.; Lee, Y.; et al. Differential effect of SARS-CoV-2 infection on stress granule formation in Vero and Calu-3 cells. *Front Microbiol* **2022**, *13*, 997539, doi:10.3389/fmicb.2022.997539.
36. Liu, H.; Bai, Y.; Zhang, X.; Gao, T.; Liu, Y.; Li, E.; Wang, X.; Cao, Z.; Zhu, L.; Dong, Q.; et al. SARS-CoV-2 N Protein Antagonizes Stress Granule Assembly and IFN Production by Interacting with G3BPs to Facilitate Viral Replication. *J Virol* **2022**, *96*, e0041222, doi:10.1128/jvi.00412-22.
37. Biswal, M.; Lu, J.; Song, J. SARS-CoV-2 Nucleocapsid Protein Targets a Conserved Surface Groove of the NTF2-like Domain of G3BP1. *J Mol Biol* **2022**, *434*, 167516, doi:10.1016/j.jmb.2022.167516.
38. Kleer, M.; Mulloy, R.P.; Robinson, C.A.; Evseev, D.; Bui-Marinos, M.P.; Castle, E.L.; Banerjee, A.; Mubareka, S.; Mossman, K.; Corcoran, J.A. Human coronaviruses disassemble processing bodies. *PLoS Pathog* **2022**, *18*, e1010724, doi:10.1371/journal.ppat.1010724.
39. Strong, M.J. The evidence for altered RNA metabolism in amyotrophic lateral sclerosis (ALS). *J. Neurol. Sci* **2010**, *288*, 1-12.
40. Aulas, A.; Vande, V.C. Alterations in stress granule dynamics driven by TDP-43 and FUS: a link to pathological inclusions in ALS? *Front Cell Neurosci* **2015**, *9*, 423, doi:10.3389/fncel.2015.00423 [doi].

41. Keller, B.A.; Volkening, K.; Droppelmann, C.A.; Ang, L.C.; Rademakers, R.; Strong, M.J. Co-aggregation of RNA binding proteins in ALS spinal motor neurons: evidence of a common pathogenic mechanism. *Acta Neuropathol* **2012**, *124*, 733-747, doi:10.1007/s00401-012-1035-z [doi].
42. Abramson, J.; Adler, J.; Dunger, J.; Evans, R.; Green, T.; Pritzel, A.; Ronneberger, O.; Willmore, L.; Ballard, A.J.; Bambrick, J.; et al. Accurate structure prediction of biomolecular interactions with AlphaFold 3. *Nature* **2024**, *630*, 493-500, doi:10.1038/s41586-024-07487-w.
43. Drino, A.; Schaefer, M.R. RNAs, Phase Separation, and Membrane-Less Organelles: Are Post-Transcriptional Modifications Modulating Organelle Dynamics? *Bioessays* **2018**, *40*, e1800085, doi:10.1002/bies.201800085.
44. Wiedner, H.J.; Giudice, J. It's not just a phase: function and characteristics of RNA-binding proteins in phase separation. *Nat Struct Mol Biol* **2021**, *28*, 465-473, doi:10.1038/s41594-021-00601-w.
45. Gotor, N.L.; Armaos, A.; Calloni, G.; Torrent Burgas, M.; Vabulas, R.M.; De Groot, N.S.; Tartaglia, G.G. RNA-binding and prion domains: the Yin and Yang of phase separation. *Nucleic Acids Res* **2020**, *48*, 9491-9504, doi:10.1093/nar/gkaa681.
46. Hofweber, M.; Dormann, D. Friend or foe-Post-translational modifications as regulators of phase separation and RNP granule dynamics. *J Biol Chem* **2019**, *294*, 7137-7150, doi:10.1074/jbc.TM118.001189.
47. Fakim, H.; Vande Velde, C. The implications of physiological biomolecular condensates in amyotrophic lateral sclerosis. *Semin Cell Dev Biol* **2024**, *156*, 176-189, doi:10.1016/j.semcdb.2023.05.006.
48. Wang, J.; Choi, J.M.; Holehouse, A.S.; Lee, H.O.; Zhang, X.; Jahnel, M.; Maharana, S.; Lemaitre, R.; Pozniakovsky, A.; Drechsel, D.; et al. A Molecular Grammar Governing the Driving Forces for Phase Separation of Prion-like RNA Binding Proteins. *Cell* **2018**, *174*, 688-699 e616, doi:10.1016/j.cell.2018.06.006.
49. Giambruno, R.; Grzybowska, E.A.; Fawzi, N.L.; Dormann, D. Editorial: The Role of Protein Post-Translational Modifications in Protein-RNA Interactions and RNP Assemblies. *Front Mol Biosci* **2021**, *8*, 831810, doi:10.3389/fmolb.2021.831810.
50. England, W.E.; Wang, J.; Chen, S.; Baldi, P.; Flynn, R.A.; Spitale, R.C. An atlas of posttranslational modifications on RNA binding proteins. *Nucleic Acids Res* **2022**, *50*, 4329-4339, doi:10.1093/nar/gkac243.
51. Velazquez-Cruz, A.; Banos-Jaime, B.; Diaz-Quintana, A.; De la Rosa, M.A.; Diaz-Moreno, I. Post-translational Control of RNA-Binding Proteins and Disease-Related Dysregulation. *Front Mol Biosci* **2021**, *8*, 658852, doi:10.3389/fmolb.2021.658852.
52. Corley, M.; Burns, M.C.; Yeo, G.W. How RNA-Binding Proteins Interact with RNA: Molecules and Mechanisms. *Mol Cell* **2020**, *78*, 9-29, doi:10.1016/j.molcel.2020.03.011.
53. Zhao, B.; Katuwawala, A.; Oldfield, C.J.; Hu, G.; Wu, Z.; Uversky, V.N.; Kurgan, L. Intrinsic Disorder in Human RNA-Binding Proteins. *J Mol Biol* **2021**, *433*, 167229, doi:10.1016/j.jmb.2021.167229.
54. Harrison, A.F.; Shorter, J. RNA-binding proteins with prion-like domains in health and disease. *Biochem J* **2017**, *474*, 1417-1438, doi:10.1042/BCJ20160499.
55. Banani, S.F.; Lee, H.O.; Hyman, A.A.; Rosen, M.K. Biomolecular condensates: organizers of cellular biochemistry. *Nat Rev Mol Cell Biol* **2017**, *18*, 285-298, doi:10.1038/nrm.2017.7.
56. Li, L.; McGinnis, J.P.; Si, K. Translational Control by Prion-like Proteins. *Trends Cell Biol* **2018**, *28*, 494-505, doi:10.1016/j.tcb.2018.02.002.
57. Hentze, M.W.; Castello, A.; Schwarzl, T.; Preiss, T. A brave new world of RNA-binding proteins. *Nat Rev Mol Cell Biol* **2018**, *19*, 327-341, doi:10.1038/nrm.2017.130.
58. Wadsworth, G.M.; Zahurancik, W.J.; Zeng, X.; Pullara, P.; Lai, L.B.; Sidharthan, V.; Pappu, R.V.; Gopalan, V.; Banerjee, P.R. RNAs undergo phase transitions with lower critical solution temperatures. *Nat Chem* **2023**, *15*, 1693-1704, doi:10.1038/s41557-023-01353-4.
59. Levine, K.S.; Leonard, H.L.; Blauwendraat, C.; Iwaki, H.; Johnson, N.; Bandres-Ciga, S.; Ferrucci, L.; Faghri, F.; Singleton, A.B.; Nalls, M.A. Virus exposure and neurodegenerative disease risk across national biobanks. *Neuron* **2023**, *111*, 1086-1093 e1082, doi:10.1016/j.neuron.2022.12.029.
60. Piekut, T.; Hurla, M.; Banaszek, N.; Szejn, P.; Dorszewska, J.; Kozubski, W.; Prendecki, M. Infectious agents and Alzheimer's disease. *J Integr Neurosci* **2022**, *21*, 73, doi:10.31083/j.jin2102073.
61. Badrfam, R.; Zandifar, A. From encephalitis lethargica to COVID-19: Is there another epidemic ahead? *Clin Neurol Neurosurg* **2020**, *196*, 106065, doi:10.1016/j.clineuro.2020.106065.
62. Matschke, J.; Lutgehetmann, M.; Hagel, C.; Sperhake, J.P.; Schroder, A.S.; Edler, C.; Mushumba, H.; Fitzek, A.; Allweiss, L.; Dandri, M.; et al. Neuropathology of patients with COVID-19 in Germany: a post-mortem case series. *Lancet Neurol* **2020**, *19*, 919-929, doi:10.1016/S1474-4422(20)30308-2.
63. Stein, S.R.; Ramelli, S.C.; Grazioli, A.; Chung, J.Y.; Singh, M.; Yinda, C.K.; Winkler, C.W.; Sun, J.; Dickey, J.M.; Ylaya, K.; et al. SARS-CoV-2 infection and persistence in the human body and brain at autopsy. *Nature* **2022**, *612*, 758-763, doi:10.1038/s41586-022-05542-y.
64. Song, E.; Zhang, C.; Israelow, B.; Lu-Culligan, A.; Prado, A.V.; Skriabine, S.; Lu, P.; Weizman, O.E.; Liu, F.; Dai, Y.; et al. Neuroinvasion of SARS-CoV-2 in human and mouse brain. *J Exp Med* **2021**, *218*, doi:10.1084/jem.20202135.

65. Emmi, A.; Rizzo, S.; Barzon, L.; Sandre, M.; Carturan, E.; Sinigaglia, A.; Riccetti, S.; Della Barbera, M.; Boscolo-Berto, R.; Cocco, P.; et al. Detection of SARS-CoV-2 viral proteins and genomic sequences in human brainstem nuclei. *NPJ Parkinsons Dis* **2023**, *9*, 25, doi:10.1038/s41531-023-00467-3.
66. Mukerji, S.S.; Solomon, I.H. What can we learn from brain autopsies in COVID-19? *Neurosci Lett* **2021**, *742*, 135528, doi:10.1016/j.neulet.2020.135528.
67. Thakur, K.T.; Miller, E.H.; Glendinning, M.D.; Al-Dalahmah, O.; Banu, M.A.; Boehme, A.K.; Boubour, A.L.; Bruce, S.S.; Chong, A.M.; Claassen, J.; et al. COVID-19 neuropathology at Columbia University Irving Medical Center/New York Presbyterian Hospital. *Brain* **2021**, *144*, 2696-2708, doi:10.1093/brain/awab148.
68. Lee, M.H.; Perl, D.P.; Steiner, J.; Pasternack, N.; Li, W.; Maric, D.; Safavi, F.; Horkayne-Szakaly, I.; Jones, R.; Stram, M.N.; et al. Neurovascular injury with complement activation and inflammation in COVID-19. *Brain* **2022**, *145*, 2555-2568, doi:10.1093/brain/awac151.
69. Lebrun, L.; Absil, L.; Remmelink, M.; De Mendonca, R.; D'Haene, N.; Gaspard, N.; Rusu, S.; Racu, M.L.; Collin, A.; Allard, J.; et al. SARS-Cov-2 infection and neuropathological findings: a report of 18 cases and review of the literature. *Acta Neuropathol Commun* **2023**, *11*, 78, doi:10.1186/s40478-023-01566-1.
70. Sun, Y.; Abriola, L.; Niederer, R.O.; Pedersen, S.F.; Alfajaro, M.M.; Silva Monteiro, V.; Wilen, C.B.; Ho, Y.C.; Gilbert, W.V.; Surovtseva, Y.V.; et al. Restriction of SARS-CoV-2 replication by targeting programmed -1 ribosomal frameshifting. *Proc Natl Acad Sci U S A* **2021**, *118*, doi:10.1073/pnas.2023051118.
71. Schurink, B.; Roos, E.; Radonic, T.; Barbe, E.; Bouman, C.S.C.; de Boer, H.H.; de Bree, G.J.; Bulle, E.B.; Aronica, E.M.; Florquin, S.; et al. Viral presence and immunopathology in patients with lethal COVID-19: a prospective autopsy cohort study. *Lancet Microbe* **2020**, *1*, e290-e299, doi:10.1016/S2666-5247(20)30144-0.
72. Yang, A.C.; Kern, F.; Losada, P.M.; Agam, M.R.; Maat, C.A.; Schmartz, G.P.; Fehlmann, T.; Stein, J.A.; Schaum, N.; Lee, D.P.; et al. Dysregulation of brain and choroid plexus cell types in severe COVID-19. *Nature* **2021**, *595*, 565-571, doi:10.1038/s41586-021-03710-0.
73. Jacomy, H.; Fragoso, G.; Almazan, G.; Mushynski, W.E.; Talbot, P.J. Human coronavirus OC43 infection induces chronic encephalitis leading to disabilities in BALB/C mice. *Virology* **2006**, *349*, 335-346, doi:10.1016/j.virol.2006.01.049.
74. Cappelletti, G.; Colombrita, C.; Limanaqi, F.; Invernizzi, S.; Garziano, M.; Vanetti, C.; Moscheni, C.; Santangelo, S.; Zecchini, S.; Trabattoni, D.; et al. Human motor neurons derived from induced pluripotent stem cells are susceptible to SARS-CoV-2 infection. *Front Cell Neurosci* **2023**, *17*, 1285836, doi:10.3389/fncel.2023.1285836.
75. Philippens, I.; Boszormenyi, K.P.; Wubben, J.A.M.; Fagrouch, Z.C.; van Driel, N.; Mayenburg, A.Q.; Lozovagia, D.; Roos, E.; Schurink, B.; Bugiani, M.; et al. Brain Inflammation and Intracellular alpha-Synuclein Aggregates in Macaques after SARS-CoV-2 Infection. *Viruses* **2022**, *14*, doi:10.3390/v14040776.
76. Wu, Z.; Zhang, X.; Huang, Z.; Ma, K. SARS-CoV-2 Proteins Interact with Alpha Synuclein and Induce Lewy Body-like Pathology In Vitro. *Int J Mol Sci* **2022**, *23*, doi:10.3390/ijms23063394.
77. Semerdzhiev, S.A.; Fakhree, M.A.A.; Segers-Nolten, I.; Blum, C.; Claessens, M. Interactions between SARS-CoV-2 N-Protein and alpha-Synuclein Accelerate Amyloid Formation. *ACS Chem Neurosci* **2022**, *13*, 143-150, doi:10.1021/acschemneuro.1c00666.
78. Zilio, G.; Masato, A.; Sandre, M.; Caregnato, A.; Moret, F.; Maciola, A.K.; Antonini, A.; Brucale, M.; Cendron, L.; Plotegher, N.; et al. SARS-CoV-2-Mimicking Pseudoviral Particles Accelerate alpha-Synuclein Aggregation In Vitro. *ACS Chem Neurosci* **2024**, *15*, 215-221, doi:10.1021/acschemneuro.3c00468.
79. Proal, A.D.; VanElzakker, M.B.; Aleman, S.; Bach, K.; Boribong, B.P.; Buggert, M.; Cherry, S.; Chertow, D.S.; Davies, H.E.; Dupont, C.L.; et al. SARS-CoV-2 reservoir in post-acute sequelae of COVID-19 (PASC). *Nat Immunol* **2023**, *24*, 1616-1627, doi:10.1038/s41590-023-01601-2.
80. Peluso, M.J.; Deeks, S.G.; Mustapic, M.; Kapogiannis, D.; Henrich, T.J.; Lu, S.; Goldberg, S.A.; Hoh, R.; Chen, J.Y.; Martinez, E.O.; et al. SARS-CoV-2 and Mitochondrial Proteins in Neural-Derived Exosomes of COVID-19. *Ann Neurol* **2022**, *91*, 772-781, doi:10.1002/ana.26350.
81. Crunfli, F.; Carregari, V.C.; Veras, F.P.; Silva, L.S.; Nogueira, M.H.; Antunes, A.; Vendramini, P.H.; Valenca, A.G.F.; Brandao-Teles, C.; Zuccoli, G.D.S.; et al. Morphological, cellular, and molecular basis of brain infection in COVID-19 patients. *Proc Natl Acad Sci U S A* **2022**, *119*, e2200960119, doi:10.1073/pnas.2200960119.
82. Gordon, D.E.; Jang, G.M.; Bouhaddou, M.; Xu, J.; Obernier, K.; White, K.M.; O'Meara, M.J.; Rezelj, V.V.; Guo, J.Z.; Swaney, D.L.; et al. A SARS-CoV-2 protein interaction map reveals targets for drug repurposing. *Nature* **2020**, *583*, 459-468, doi:10.1038/s41586-020-2286-9.
83. Vu, L.; Ghosh, A.; Tran, C.; Tebung, W.A.; Sidibe, H.; Garcia-Mansfield, K.; David-Dirgo, V.; Sharma, R.; Pirrotte, P.; Bowser, R.; et al. Defining the Caprin-1 Interactome in Unstressed and Stressed Conditions. *J Proteome Res* **2021**, *20*, 3165-3178, doi:10.1021/acs.jproteome.1c00016.
84. Bakkar, N.; Kovalik, T.; Lorenzini, I.; Spangler, S.; Lacoste, A.; Sponaugle, K.; Ferrante, P.; Argentinis, E.; Sattler, R.; Bowser, R. Artificial intelligence in neurodegenerative disease research: use of IBM Watson to identify additional RNA-binding proteins altered in amyotrophic lateral sclerosis. *Acta Neuropathol* **2018**, *135*, 227-247, doi:10.1007/s00401-017-1785-8.

 doi:10.20944/preprints202407.0408.v1

85. Pulst, S.M.; Scoles, D.R.; Paul, S. Effects of STAU1/staufen1 on autophagy in neurodegenerative diseases. *Autophagy* **2023**, *19*, 2607-2608, doi:10.1080/15548627.2023.2169306.
86. Somasekharan, S.P.; Gleave, M. SARS-CoV-2 nucleocapsid protein interacts with immunoregulators and stress granules and phase separates to form liquid droplets. *FEBS Lett* **2021**, *595*, 2872-2896, doi:10.1002/1873-3468.14229.
87. Droppelmann, C.A.; Campos-Melo, D.; Noches, V.; McLellan, C.; Szabla, R.; Lyons, T.A.; Amzil, H.; Withers, B.; Kaplanis, B.; Sonkar, K.S.; et al. Mitigation of TDP-43 toxic phenotype by an RGNEF fragment in amyotrophic lateral sclerosis models. *Brain* **2024**, *147*, 2053-2068, doi:10.1093/brain/awae078.